Title	Simulation, measurement, and mitigation of beam instability caused by the kicker impedance in the 3-GeV rapid cycling synchrotron at the Japan Proton Accelerator Research Complex
Author(s)	Saha P. K., Shobuda Yoshihiro, Hotchi Hideaki, Harada Hiroyuki, Hayashi Naoki, Kinsho Michikazu, Tamura Fumihiko, Tani Norio, Yamamoto Masanobu, Watanabe Yasuhiro, Chin Y. H., Holmes J. A.
Citation	Physical Review Accelerators and Beams,21(2). p.024203_1-024203_20
Text Version	Published Journal Article
URL	https://jopss.jaea.go.jp/search/servlet/search?5061648
DOI	https://doi.org/10.1103/PhysRevAccelBeams.21.024203
Right	Published by the American Physical Society under the terms of the Creative Commons Attribution 4.0 International license. Further distribution of this work must maintain attribution to the author(s) and the published article's title, journal citation, and DOI.

Simulation, measurement, and mitigation of beam instability caused by the kicker impedance in the 3-GeV rapid cycling synchrotron at the Japan Proton Accelerator Research Complex

P. K. Saha,* Y. Shobuda, H. Hotchi, H. Harada, N. Hayashi, M. Kinsho, F. Tamura, N. Tani, M. Yamamoto, and Y. Watanabe

Accelerator division, J-PARC center, Japan Atomic Energy Agency (JAEA), 2-4 Shirakata, Tokai-mura, Naka-gun, Ibaraki 319-1195, Japan

Yong Ho Chin

High Energy Accelerator Research Organization (KEK), Tsukuba, Ibaraki 305-0801, Japan

J. A Holmes

Spallation Neutron Source, Oak Ridge, Tennessee, USA

(Received 26 December 2016; published 14 February 2018)

The transverse impedance of eight extraction pulsed kicker magnets is a strong beam instability source in the 3-GeV rapid cycling synchrotron (RCS) at the Japan Proton Accelerator Research Complex. Significant beam instability occurs even at half of the designed 1 MW beam power when the chromaticity (ξ) is fully corrected for the entire acceleration cycle by using ac sextupole (SX) fields. However, if ξ is fully corrected only at the injection energy by using dc SX fields, the beam is stable. In order to study realistic beam instability scenarios, including the effect of space charge and to determine practical measures to accomplish 1 MW beam power, we enhance the ORBIT particle tracking code to incorporate all realistic time-dependent machine parameters, including the time dependence of the impedance itself. The beam stability properties beyond 0.5 MW beam power are found to be very sensitive to a number of parameters in both simulations and measurements. In order to stabilize a beam at 1 MW beam power, two practical measures based on detailed and systematic simulation studies are determined, namely, (i) proper manipulation of the betatron tunes during acceleration and (ii) reduction of the dc SX field to reduce the ξ correction even at injection. The simulation results are well reproduced by measurements, and, as a consequence, an acceleration to 1 MW beam power is successfully demonstrated. In this paper, details of the ORBIT simulation and the corresponding experimental results up to 1 MW of beam power are presented. To further increase the RCS beam power, beam stability issues and possible measures beyond 1 MW beam power are also considered.

DOI: 10.1103/PhysRevAccelBeams.21.024203

I. INTRODUCTION

The 3-GeV rapid cycling synchrotron (RCS) in the Japan Proton Accelerator Research Complex (J-PARC) acts as a high-intensity proton beam source for the neutron and muon production targets in the Material and Life Science Experimental Facility (MLF), as well as the injector for the main ring synchrotron (MR) [1]. The designed extracted beam power of the RCS is as high as 1 MW, which corresponds to 8.33×10^{13} protons per pulse (ppp) in two bunches. The beam energy at injection has recently been upgraded from an initial value of 0.181 GeV to the designed value of 0.4 GeV. The beam is then accelerated up to 3 GeV in the RCS and delivered simultaneously to the MLF and MR at a repetition rate of 25 Hz. The production beam power for the user operation so far has reached 0.5 MW, but systematic studies have been performed at power levels up to the designed beam power [2].

Figure 1 shows a schematic view of the RCS. The RCS has a threefold symmetric lattice with three arcs and three long straight sections and a circumference of 348.333 m. The H^- charge exchange injection and the beam collimation systems are placed in the first straight section, while the beam extraction and the rf systems are placed in the second and third straight sections, respectively.

The key parameters of the RCS, especially those related to the present article, are summarized in Table I.

*Corresponding author.
saha.pranab@j-parc.jp

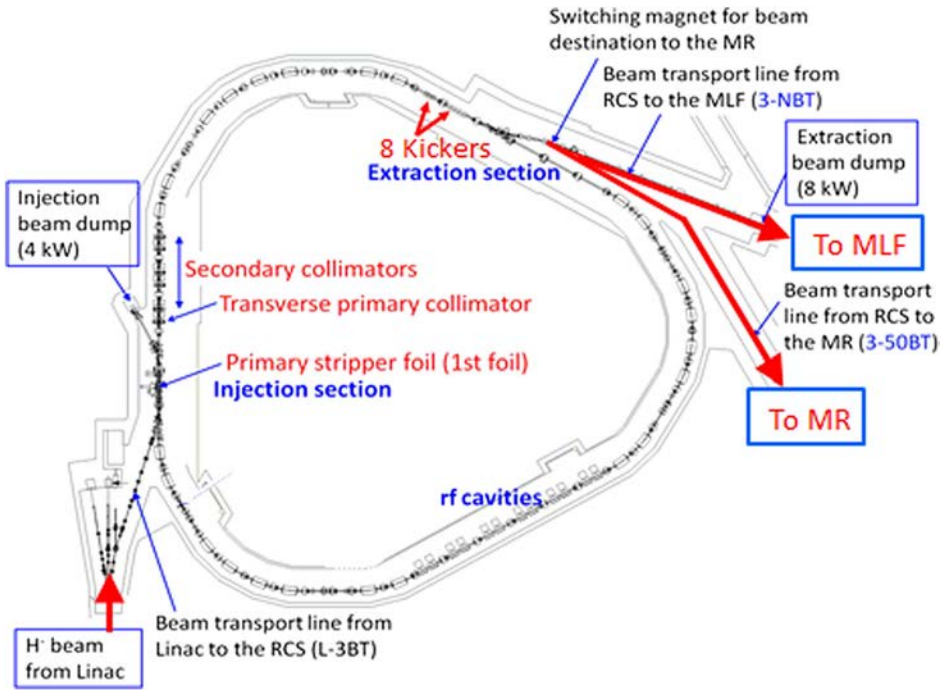

FIG. 1. Schematic view of 3-GeV RCS at J-PARC. The eight pulsed kicker magnets (KMs) placed in the second straight (extraction) section are used for beam extraction. The extracted beam is delivered simultaneously to the MLF and MR. The transverse impedance of the KMs is a strong source of beam instability in the RCS.

The time-independent parameters are given in the upper half, while time-dependent ones are listed in the bottom half of the table. Details about RCS parameters can be found in the J-PARC technical design report [1].

TABLE I. Main parameters of the RCS [1]. The time-independent and time-dependent parameters are separated into the upper and lower halves of the table, respectively.

Name	Value
Circumference [m]	348.333
Transition energy [GeV]	9
Repetition rate [Hz]	25
Harmonic number (h)	2
Number of bunches	2
Number of protons per pulse (ppp)	8.33×10^{13}
Output beam power [MW]	1
Average beta function $\langle\beta_x\rangle\langle\beta_y\rangle$ [m]	11.6, 11.9
$\Delta p/p$ acceptance [%]	1
Natural chromaticity (ξ_x, ξ_y)	−10, −7

Name	Injection	Extraction
Kinetic energy [GeV]	0.4	3
Revolution frequency (f_0) [MHz]	0.614	0.84
Betatron tunes (ν_x, ν_y)	(6.45, 6.42)	(6.399, 6.405)
Synchrotron tune (ν_s)	0.0053	0.0005
Slippage factor (η)	−0.478	−0.047
Momentum spread ($\Delta p/p$) [99%]	0.8	0.4
Bunch length [m]	160	60
Bunching factor (B_f)	0.47	0.21

Beam instability is always a big concern for a beam of intensity as high as 1 MW. In the design stage, sources of beam instability throughout the machine were addressed carefully, and the transverse horizontal impedance of the eight pulsed extraction magnets (KMs) was found to be the dominant driver of beam instability in the RCS [3–5]. Compared to a similar high-intensity machine, the impedance of the RCS KMs is nearly one order of magnitude higher than that of the kicker magnets in the Spallation Neutron Source in Oak Ridge [6]. It is worth mentioning that in the RCS alumina ceramics vacuum chambers has been installed. The chambers have titanium flanges and an exterior rf shield to reduce the duct impedance. The TiN coating has also been done in the inner surface of the ducts to suppress secondary electron emission [7,8]. The transverse wall impedance Z_x can be expressed as $\sim\frac{jLZ_0}{2\pi\beta\gamma^2}\frac{1}{\rho^2}$ [9], where L is the circumference of the RCS, Z_0 is the impedance of free space (377 Ω), ρ is the average radius of the vacuum chamber (0.145 m), and β and γ are relativistic parameters. The Z_x for the RCS is estimated to be $\sim j9.94 \times 10^5/\beta\gamma^2$ [Ω/m].

Recently, a direct measure to reduce the KM impedance was proposed and also demonstrated experimentally [5,10], but practical implementation will require extensive R&D to ensure that the modified KMs can extract the beam without any problem. Unfortunately, thus far, there has been little progress in that direction. Moreover, previous studies on the severity of the KM impedance and the development of alternative measures, such as the optimization of machine

TABLE II. Incoherent tune shift $\Delta\nu_{\mathrm{incoh}}$ at injection and extraction energies estimated by using Eq. (1) for the beam intensities considered in the present study. The measured rms momentum spreads ($\Delta p/p$) of the injected beam used in the simulations are also given.

				B_f		$\Delta\nu_{\mathrm{incoh}}$	
E_{inj} [GeV]	E_{ext} [GeV]	$\Delta p/p$ [%]	N ($\times 10^{13}$)	(Inj)	(Ext)	(Inj)	(Ext)
0.181	3	0.08	3.124	0.45	0.16	−0.34	−0.04
0.181	3	0.08	4.165	0.45	0.16	−0.45	−0.06
0.4	3	0.08	4.165	0.45	0.18	−0.15	−0.03
0.4	3	0.08	6.248	0.45	0.18	−0.23	−0.05
0.4	3	0.18	6.248	0.47	0.21	−0.22	−0.04
0.4	3	0.18	8.33	0.47	0.21	−0.29	−0.05

and beam parameters, to stabilize the beam at the designed 1 MW beam power are inadequate. Given the impedances, one can generally estimate the beam instability threshold by calculating the growth rate of the beam instability. This depends on many parameters, of which the beam intensity, chromaticity, and betatron tunes are the most significant [11]. However, in synchrotrons, one needs to cope with many detailed time-dependent machine parameters, error sources, and impedances. Therefore, a precise numerical simulation that considers the details of these variations as well as the effects of space charge and other beam instability sources is required.

The effect of space charge on beam instabilities has been studied theoretically and discussed intensively by many authors [12–19], and a short summary of their findings appears in Ref. [20]. By taking into account only the direct space charge effect and in a moderate space charge regime defined by the ratio of the space charge tune shift to the synchrotron tune ($\Delta\nu/\nu_s$), Balbekov [15] considered the general problem in the limit that the instability growth rate is small compared to the synchrotron and space charge frequency shifts. Balbekov's main conclusion is that the space charge tune spread causes significant Landau damping which suppresses most transverse modes. Recently, Balbekov has also shown that the threshold of the transverse mode coupling instability increases with increasing the space charge parameter, and the threshold is not limited up to the moderate space charge regime, but also with $\Delta\nu/\nu_s$ far exceeding the unity [19]. In the present work, we studied with dynamic variations of the RCS parameters, injected beam parameters, and also the beam intensity, which eventually give a scope to study in a wide range of the space charge regime or the above space charge parameter $\Delta\nu/\nu_s$. Although these theoretical studies can provide significant insight into the dynamical effects of space charge on beam stability, the detailed study of beam stability in a complicated scenario, such as acceleration in the RCS, demands a simulation approach.

To assess the magnitude of the space charge force in the RCS, we consider the incoherent space charge tune shift, known also as the Laslett incoherent tune shift ($\Delta\nu_{\mathrm{incoh}}$). For a bunched beam, the $\Delta\nu_{\mathrm{incoh}}$ can be simply expressed, neglecting wall effects, as [21]

$$\Delta\nu_{\mathrm{incoh}} = -\frac{N r_p}{2\pi\beta^2\gamma^3\epsilon}\frac{1}{B_f}, \tag{1}$$

where N is the number of particles in the ring, r_p is the classical radius of the proton (1.54×10^{-18} m), β (0.713) and γ (1.4263 MeV) are the relativistic parameters of the beam, ϵ is the transverse emittance (which is 100π mm mrad at injection energy in the RCS), and B_f is the bunching factor, defined by the ratio of the average beam current to the peak beam current. The bunching factor is typically kept at more than 0.4 at the injection energy by applying dual harmonic rf voltages and longitudinal injection painting.

The incoherent space charge tune shift according to Eq. (1) increases at lower beam energies due to the $\beta^2\gamma^3$ factor, while it is also worth mentioning that the direct space charge tune shift also increases on the beam energy similarly by a factor of $\beta\gamma^2$. The effect of space charge effect in the RCS is very significant not only because of the 1 MW beam power but also because of the low injection energy of 0.4 GeV. For example, the value of $\Delta\nu_{\mathrm{incoh}}$ obtained by using Eq. (1) is estimated to be as high as −0.29 at injection energy. In this estimation, a bunching factor of 0.47 and transverse emittance $\epsilon = 100\pi$ mm mrad are assumed.

Table II gives a summary of $\Delta\nu_{\mathrm{incoh}}$ estimated using Eq. (1), at injection and extraction for the beam intensities considered in the present study. The values of $\Delta\nu_{\mathrm{incoh}}$ are estimated for both the previous and the present injection energies of 0.181 and 0.4 GeV, respectively, as well as for the extraction energy of 3 GeV.

In a similar way, the coherent betatron tune shift ($\Delta\nu_{\mathrm{coh}}$) for the bunched beam, shown here for the vertical plane, can be expressed as [21,22]

$$\Delta\nu_{\mathrm{coh}} = -\frac{N r_p\langle\beta_y\rangle}{\pi\gamma}\left[\left(\frac{1}{\beta^2\gamma^2 B_f}+1\right)\frac{\xi_1}{\rho^2}+\mathcal{F}\frac{\xi_2}{h^2}\right], \tag{2}$$

TABLE III. Estimated values of coherent tune shift $\Delta\nu_{\mathrm{coh}}$ at injection and extraction energies using Eq. (2) for the beam intensities considered in the present study. The measured rms momentum spreads ($\Delta p/p$) of the injected beam used in the simulations are also given.

				B_f		$\Delta\nu_{\mathrm{coh}}$	
E_{inj} [GeV]	E_{ext} [GeV]	$\Delta p/p$ [%]	N ($\times 10^{13}$)	(Inj)	(Ext)	(Inj)	(Ext)
0.181	3	0.08	3.124	0.45	0.16	−0.025	−0.002
0.181	3	0.08	4.165	0.45	0.16	−0.033	−0.003
0.4	3	0.08	4.165	0.45	0.18	−0.015	−0.003
0.4	3	0.08	6.248	0.45	0.18	−0.023	−0.004
0.4	3	0.18	6.248	0.47	0.21	−0.022	−0.004
0.4	3	0.18	8.33	0.47	0.21	−0.030	−0.005

where $\langle\beta_y\rangle$ is the average vertical betatron function of the ring, ξ_1 and ξ_2 are Laslett coefficients, which depend on the shape of the vacuum chamber, ρ is half the vertical height of the vacuum chamber, which is taken to be a conducting boundary in this simulation, and h is half the vertical gap between magnet pole faces, which is set equal to ρ here. The vacuum chamber is circular for our case, and thus ρ is the radius of the vacuum chamber, which is 0.145 m. $\mathcal{F}$ is the fraction of the vacuum chamber with magnet pole faces, which is considered to be 0.5. The values of ξ_1 and ξ_2 are given to be 0.5 and 0.617, respectively [21]. The value $\langle\beta_y\rangle$ for the present betatron tune is calculated to be 11.9 m. As with $\Delta\nu_{\mathrm{incoh}}$, the value of $\Delta\nu_{\mathrm{coh}}$ decreases with increasing beam energy in synchrotrons, but the reduction factor is $1/\gamma$. Regardless of the transverse beam size, the coherent tune shift is inversely proportional to the square of the half size of the vacuum chamber.

Table III gives a summary of $\Delta\nu_{\mathrm{coh}}$ estimated for the same beam parameters as used for estimating $\Delta\nu_{\mathrm{incoh}}$ (Table II). The values of $\Delta\nu_{\mathrm{coh}}$ are found to be more than one order of magnitude smaller than $\Delta\nu_{\mathrm{incoh}}$, but they are almost a similar order of magnitude larger than the synchrotron tune (see Table I). In simulations, one can study the effect of the indirect space charge effect on multiparticle beam dynamics by changing the vacuum chamber radius.

The motivation of the present work was to study realistic beam instability scenarios in the J-PARC RCS while incorporating all relevant dynamics including the effect of the space charge. The object was to determine definite measures to accomplish the designed 1 MW beam power in the RCS. For that purpose, we used the ORBIT 3D particle tracking code with space charge, which has incorporated many time-dependent quantities to make it capable of detailed beam simulations in synchrotrons [23]. The basic models in the ORBIT code are described in Ref. [24], and detailed descriptions of the space charge and impedance models used here are presented in Ref. [20]. In order to perform realistic simulations of the RCS, we introduced numerous enhancements to the code to cope with all relevant time-dependent machine parameters and error sources, as well as realistic transverse and longitudinal injection painting. We also upgraded the impedance model to incorporate realistic time-dependent impedances for the beam instability simulation. As a result, we obtained simulations in agreement with experimental results at the then maximum beam power of 0.5 MW. These found that beam instability occurs only when the chromaticity (ξ) is fully corrected for the entire acceleration cycle by using ac sextupole (SX) fields, but no beam instability occurs if ξ is fully corrected only at the injection energy by using dc SX fields.

Fortunately, the latter choice of the SX fields was adequate to maintain acceptable beam losses, which occur mainly at injection energy, and thus there were no serious issues pertaining to beam instability in RCS operation up to 0.5 MW of beam power. However, that does not guarantee that the beam will remain stable up to the designed 1 MW beam power, not only because the beam power is doubled but also because the injection energy is upgraded from 0.181 GeV to the design value 0.4 GeV. For example, the effect of space charge at injection, as seen in both $\Delta\nu_{\mathrm{coh}}$ and $\Delta\nu_{\mathrm{incoh}}$, is significantly reduced by a factor of 2 or 3 at the upgraded injection energy. In addition, the momentum spread ($\Delta p/p$) of the injected beam was 0.08% at 0.181-GeV injection energy, but it was set to be more than twice, namely, 0.18%, for 0.4-GeV injection. A wider $\Delta p/p$ leads to a reduced circulating peak beam density through a higher B_f, and the tune shift is inversely proportional to the B_f [21].

A reduction of the space charge effect (tune shift), especially at lower energies, is very beneficial for minimizing beam losses by keeping the beam away from many lattice resonances. However, the beam instability scenario would possibly be changed due to the change of the space charge effect. The situation, especially at high intensities, becomes rather complicated because of nonlinear dependence on many parameters and their coupled effects. Accordingly, systematic simulation studies were carried out to study the detailed beam instability scenarios at 1 MW beam power, as well as to determine realistic parameters by which beam instabilities can be suppressed completely. The simulation results were well reproduced by measurements, and an acceleration to 1 MW beam power has also been successfully demonstrated.

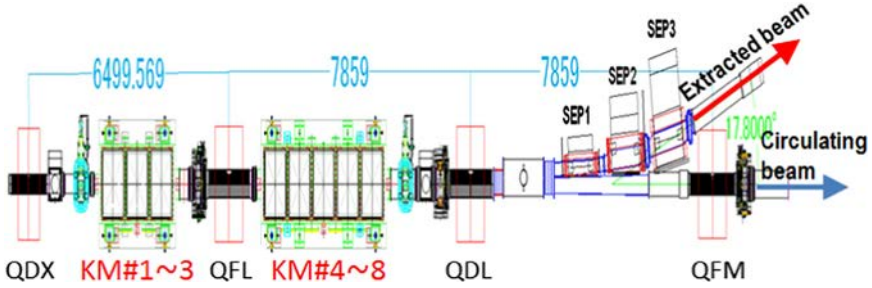

FIG. 2. Layout of the RCS extraction straight section. A total of eight pulsed kicker magnets is used for the beam extraction. The first three are placed upstream of a horizontally focusing quadrupole magnet (QFL), while the other five are placed downstream of the QFL. The transverse impedance of the kicker magnets is the dominant source of beam instability in the RCS.

II. RCS KICKER MAGNETS AND THEIR TRANSVERSE IMPEDANCES

Figure 2 shows a schematic view of the RCS extraction area, where eight pulsed kicker magnets (KMs 1–8) have been placed for beam extraction. Fast extraction is performed by these eight KMs followed by three dc extraction septum magnets (ESEPs 1–3). The two circulating bunches of the beam at the top energy of 3 GeV (each typically 200 ns long and 600 ns apart each other) are kicked out horizontally, first by the KM system and then by the ESEPs to accomplish the extraction. A detailed description of the configuration of the KMs, their power supplies, and their working principle can be found in Ref. [25]. Here, we list only a few key parameters. The longitudinal length and the gap width of all magnets are the same at 0.638 and 0.280 m, respectively, but they fall into three different classes categorized by gap height as small (S), medium (M), and large (L). The gap heights of the S type (KMs 3–5), M type (KMs 2 and 6), and L type (KMs 1, 7, and 8) are 0.153, 0.173, and 0.199 m, respectively.

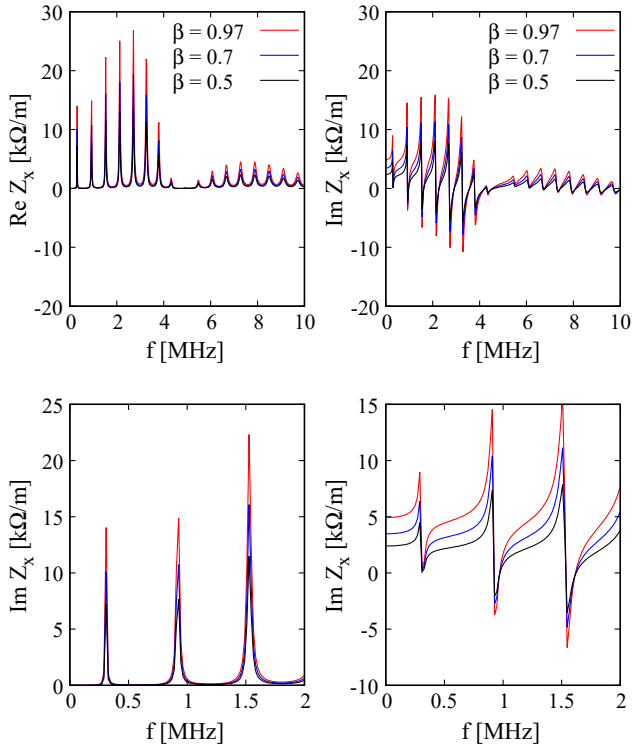

FIG. 3. Real (left) and imaginary (right) parts of theoretically given transverse impedances of a KM in the RCS [5]. The left and right plots show the real and the imaginary parts of the impedance, respectively. The impedance of a relativistic beam is seen to be much higher than that of a nonrelativistic beam. The expanded view of the impedances at the lower frequency region are shown in the lower plots.

Figure 3 shows the theoretical transverse horizontal impedances of one of the eight KMs in the RCS. The left and right plots are the real and the imaginary parts of the impedances, respectively [5]. The upper figures expanded in the lower frequency region are shown in the lower plots. The impedances are plotted for three different energies given in terms of Lorentz β: $\beta = 0.5$ corresponds nearly to the original 0.181-GeV injection energy; $\beta = 0.7$ corresponds to the present injection energy of 0.4 GeV; while $\beta = 0.97$ corresponds to the extraction energy of 3 GeV. The corresponding revolution frequencies are 0.47, 0.614, and 0.84 MHz, respectively. It can be easily seen that the transverse impedances of the KMs depend strongly on the Lorentz factors and that they increase in the case of a relativistic beam. The sharp peaks are the characteristic impedances of the RCS KMs, and they are caused by cable resonances of the beam-induced currents in the kicker magnets. The beam instability excited by the transverse horizontal impedances of the KMs leads to a transverse beam position growth in the horizontal plane [16].

III. ORBIT CODE ENHANCEMENT FOR REALISTIC SPACE CHARGE AND BEAM INSTABILITY SIMULATIONS IN THE RCS

To carry out realistic beam instability calculations, we first focused on performing accurate simulations of the beam losses under different rf focusing conditions that lead to different levels of space charge. This is because the effect of space charge level on beam instability has been intensively discussed recently [12,14,16–19]. However, unlike a storage ring, all parameters of the machine and beam, error

sources and impedances, are time dependent in the RCS. We accommodated this by enhancing the time-dependent capabilities of the ORBIT code beyond those described in Ref. [23]. In particular, tables of longitudinal and transverse impedances, given as functions of the frequency and beam energy, are used by ORBIT to interpolate the modal impedances at the instantaneous beam energy during the simulation. These are then used in ORBIT's FFT-based impedance modules [20] to calculate the related forces on the beam. The upgrades are quite useful for realistic beam simulations of any synchrotron in which parameters change over time. It is important to mention that the ORBIT code takes indirect space charge into account in the simulation. A conducting wall boundary, which is circular in the RCS, is used with a value (radius) of 0.145 m in the simulation. It is defined as ρ in Eq. (2), where the coherent tune shift $\Delta\nu_{\mathrm{coh}}$ is inversely proportional to the square of ρ. To check the effect of space charge on the beam stability, we have done detailed simulation studies by varying the value of ρ, and the results are given in a later section.

Figure 4 shows the ramping pattern of the sinusoidal B field of the RCS bending magnets, the corresponding kinetic energy (T) of the beam, and the change in the synchronous phase (ϕ_s) as functions of time. ORBIT is now capable of considering time-dependent, turn-by-turn, changes in any parameters upon which lattice functions, error sources, nonlinearities, or any other relevant quantities depend. The first issue to consider was the additive edge-focusing effect of the four horizontal injection dc chicane magnets, also called shift bump magnets (SBs), and the four horizontal transverse injection painting magnets [26–28]. Among them, the effect of SBs is very significant because they are placed very close to each other [29]. They induce a substantial vertical focusing perturbation, resulting in a considerable deviation of the vertical lattice functions from the design values. The maximum vertical beta modulation is as high as 30%, leading to a vertical tune deviation of nearly 0.02. Details of this study can be found in Ref. [30]. The next significant issues to implement in the code were the 100 kHz ripples in the power supply (PS) of the SB [27], the 1 kHz ripples in the PS of the main dipole magnet [31], and dc leakage fields from the extraction septum magnets [32,33]. Notably, realistic injection processes, including both transverse and longitudinal injection painting, were successfully included as well. The details of both transverse and longitudinal injection painting principles in the RCS can be found in many of our earlier articles [34–38]. Finally, the enhanced ORBIT code was used to incorporate the time-dependent KM impedances.

Figure 5 shows typical patterns of rf voltages, where V_1 and V_2 are the amplitudes of fundamental and second harmonic rf voltage, respectively. In order to reduce the effect of space charge at the lower beam energy, V_2 was applied up to first 5 ms, while it is kept 80% of V_1 for the first 1 ms. The applied dual harmonic rf voltage is expressed as

$$V_{\mathrm{rf}} = V_1 \sin\phi + V_2 \sin\{2(\phi - \phi_s)\}, \tag{3}$$

where V_1 is the amplitude of the fundamental rf voltage, V_2 is the amplitude of the second harmonic rf voltage, ϕ is the phase of the rf voltage, and ϕ_s is the synchronous phase. In addition, the phase of V_2 was swept linearly from $-100°$ to $0°$ during the injection period of 0.5 ms, which results in a rather asymmetric rf potential well. Equation (3) for the applied rf voltage is then expressed as

$$V_{\mathrm{rf}} = V_1 \sin\phi + V_2 \sin\{2(\phi - \phi_s) + \phi_2\}, \tag{4}$$

where ϕ_2 is the phase offset of V_2. In the course of longitudinal injection painting, a momentum offset of -0.2% was applied in addition to the above application of the rf voltage shown by Eq. (4). This is called "maximum longitudinal injection painting."

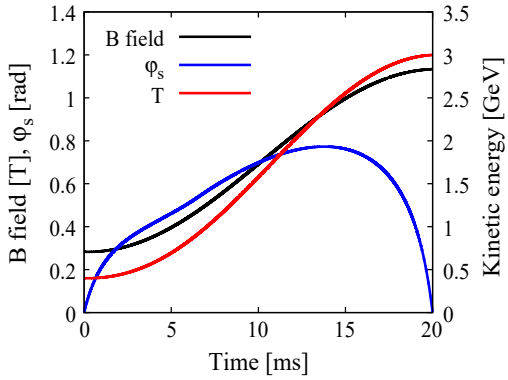

FIG. 4. Sinusoidal B field pattern of bending magnets, the corresponding kinetic energy of the beam, and the change in the synchronous phase as functions of time. Time-dependent changes in many parameters, including error sources, and kicker impedances are implemented in the present ORBIT simulations.

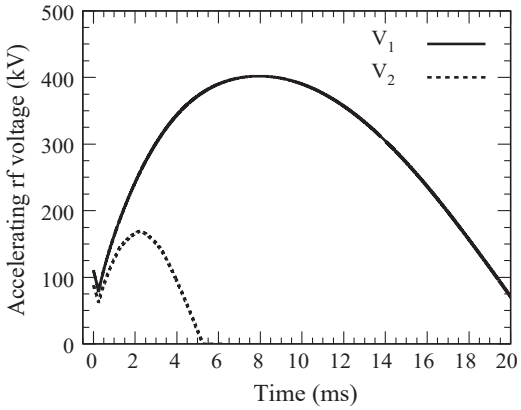

FIG. 5. The rf voltages used for RCS beam acceleration. The V_2 is applied until 5 ms from the beam injection, while it is kept 80% of V_1 for the first 1 ms, in order control the charge density of the beam and reduce the effect of space charge at a lower beam energy.

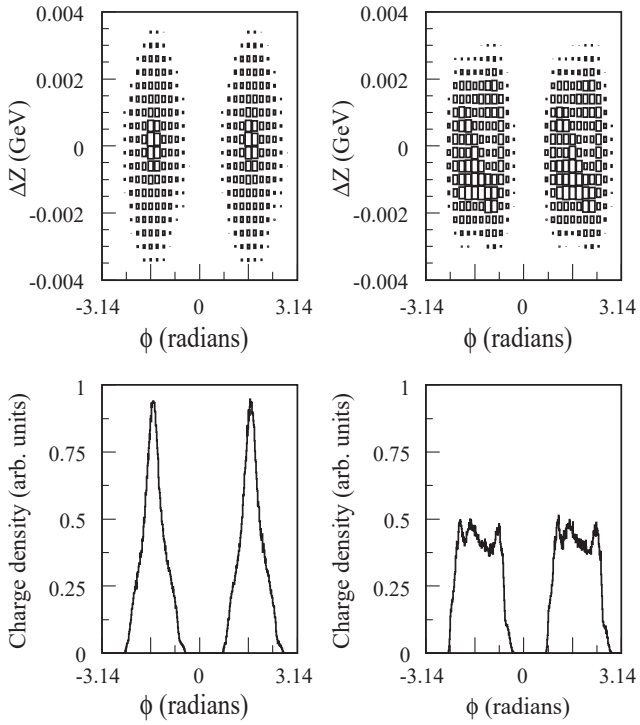

FIG. 6. Simulated longitudinal phase space distributions and their projections onto the longitudinal axis of the circulating beam at the end of injection obtained without (left) and with (right) longitudinal injection painting.

In order to consider the coupled bunch instability, a beam was injected into two bunches in the RCS simulation, just as in the machine. Figure 6 shows distributions of circulating particles on the longitudinal phase space (top) and their projections onto the longitudinal position (bottom) obtained in the simulation at the end of the 0.5 ms injection period. The horizontal axis is the longitudinal position, denoted by ϕ in radians, while the vertical axis is the energy deviation of the particles from the synchronous energy, denoted by ΔZ in GeV. The two bunches are π apart, where the circumference of the ring is defined by 2π. The plots on the left were obtained by applying only the fundamental rf voltage V_1, while the plots in the right were obtained by applying dual rf harmonic voltages ($V_1 + V_2$) and also by considering longitudinal injection painting. The peak density of the circulating beam is considerably decreased in the latter case, resulting in a bunching factor (B_f) of 0.45 at the end of injection as compared to 0.27 for the peaked bunch in the former case. However, as V_2 was applied up to only 5 ms, the subsequent values of B_f, particularly at the extraction energy, become relatively independent of the injection details, with values of about 0.2.

A. Space charge simulation results

In this subsection, we present a comparison between simulated and measured results of time-dependent beam survival studied in the presence of strong space charge at the previous injection energy of 0.181 GeV for a beam power of 0.375 MW. The effect of space charge was studied by considering the cases with and without the second harmonic rf voltage and momentum offset injection for the longitudinal injection painting.

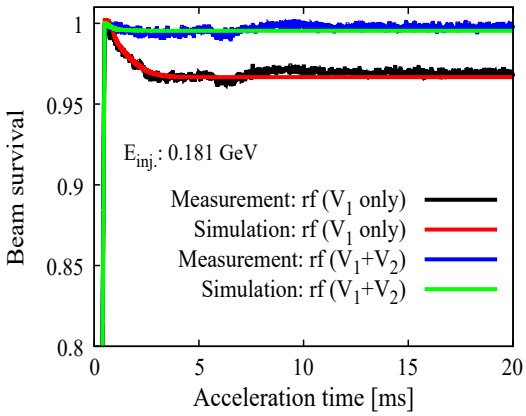

FIG. 7. Simulated and measured results of beam survival with strong and weak space charge controlled by rf patterns and longitudinal injection painting for beam power of 0.375 MW. The space-charge-induced beam loss is as high as 3% when applying only V_1, but it can be well mitigated by adding V_2 and applying longitudinal injection painting. The time structure of beam intensity loss in the simulation is shown to be consistent with the measurement results.

Figure 7 shows a comparison of beam survival between simulated and measured results for beam power of 0.375 kW (3.124×10^{13} ppp). The injection energy (E_{inj}) was 0.181 GeV, while the extraction energy was 3 GeV. A transverse injection painting emittance of 100π mm mrad was applied. The chromaticity was fully corrected only at E_{inj}, and no instability sources were considered in the simulation. The experimental data were measured using a dc current transformer placed in the first arc section of the RCS. Owing to strong space charge forces, the beam intensity was significantly attenuated by around 3% when only the fundamental rf voltage (V_1) was applied and no longitudinal injection painting was performed. However, this beam loss can be well mitigated by reducing the effect of space charge through the application of dual harmonic rf voltages ($V_1 + V_2$) and by performing longitudinal injection painting [37,38]. The time-dependent beam survival results between the simulation and the measurement were found to agree very well for both cases.

In order to understand the cause of the huge particle losses at a lower energy when applying V_1 only, we have calculated the betatron tune footprint for the two injection schemes. Figure 8 shows simulation results of betatron tune footprints by alternatively using fundamental (left) and dual (right) harmonic rf voltages (including longitudinal injection painting for the latter case) at a beam power of 0.375 MW. The top, middle, and bottom plots correspond to acceleration times of 1, 4, and 10 ms, respectively. The

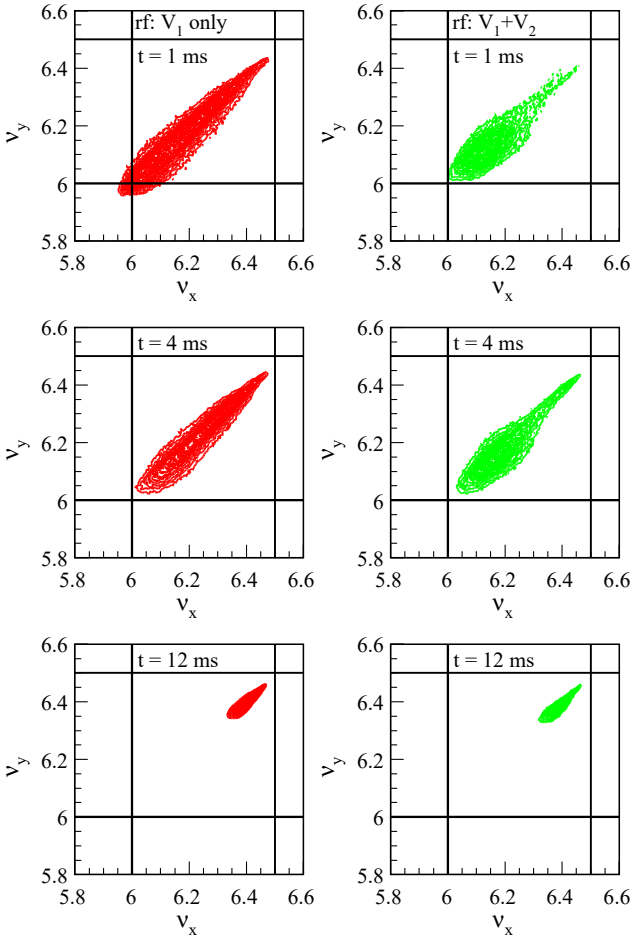

FIG. 8. Betatron tune footprints at the end of injection obtained in the simulation by using single (left) and dual (right) rf voltages for a beam power of 0.375 MW. The solid black lines are the integer and half integer resonances at $\nu_{x,y} = 6$ and $\nu_{x,y} = 6.5$, respectively.

integer resonances at $\nu_{x,y} = 6$ and half integer resonances at $\nu_{x,y} = 6.5$ are also shown by black solid lines. The space charge detuning at a low energy (top), especially when applying the rf voltage V_1 only, is much larger than that with applying both V_1 and V_2, where all order nonlinear systematic resonances are excited at $\nu_{x,y} = 6$. The particles with large tune depression suffer from emittance dilution, and those with large emittance blowup reached to the physical aperture limit and lost, which is the main reason for the significant beam loss observed at a low energy in the former case. To check in detail, we set the tunes to slightly lower and higher values than their nominal values of $\nu_{x,y} = 6.45, 6.42$. The beam survival decreases by lowering the tunes, while the beam survival increases by the other action.

On the other hand, the effect of space charge is well suppressed by applying dual harmonic rf voltages (including longitudinal injection painting), and that leads to a significant suppression of the beam loss. As the beam energy is increased during acceleration, the space charge detuning is significantly reduced [see Eq. (2)], resulting in no particle losses in the later stages of the acceleration cycle.

As shown in Table II, the bunching factor B_f at the end of the injection process was determined to be 0.45 in the latter case. At the injection energy $E_{\text{inj}} = 0.181$ GeV and 0.375 MW beam power the value of $\Delta\nu_{\text{incoh}}$ is estimated to be -0.34. It is worth mentioning that, due to $\frac{1}{\beta^2\gamma^3}$ dependence [Eq. (1)], $\Delta\nu_{\text{incoh}}$ at higher injection energy $E_{\text{inj}} = 0.4$ GeV is significantly reduced, which for the designed beam power of 1 MW yields a lower value of -0.29 than for the beam power of 0.375 MW at the lower $E_{\text{inj}} = 0.181$ GeV.

B. Implementation of kicker impedance in the ORBIT code

The implementation of impedances in the ORBIT code and the simulation of stability incorporating space charge and impedances are basically the same as already reported in Ref. [20]. However, for our purpose, we have adapted the code to ensure it considers time-dependent, turn-by-turn impedance, as the impedance changes with increasing beam energy (see Fig. 3). Instead of a constant impedance table (as for an accumulator ring), impedance tables are given as functions of relativistic β and frequency for β varying from 0.5 to 1.0 in steps of 0.05. The program generates an interpolated set of impedance values by mode number and uses those to calculate a transverse dipole kick for every turn. However, with the present version of ORBIT, the total impedance must be represented by a single node, instead of one node for each of the eight KMs in the RCS. The eight KMs are located within a span of about 8 m, and a horizontally focusing quadrupole magnet (see Fig. 2) lies between the third and the fourth KMs. We introduced the impedance node between the second and the third KMs, where the horizontal optical beta function (β_x) has a value of about 15 m. This is close to the average over the eight kickers, as shown in Fig. 9. The impedance of one KM, as shown in Fig. 3, is multiplied by 8 to account for all the KMs. All KMs are identical with equal longitudinal lengths and gap widths including their cable lengths.

IV. SEXTUPOLE STRENGTH VERSUS LATTICE CHROMATICITY

Transverse beam instability depends strongly on the degree of lattice chromaticity (ξ) correction. The ξ determines the variation of betatron tunes with respect to beam momentum variation, and it is usually defined as $\frac{\Delta\nu/\nu}{\Delta p/p}$. Generally, the beam instability growth rate can be suppressed by keeping the ξ as close as to the natural value because of enhanced Landau damping due to a large tune spread. However, ξ is usually corrected to control the spread in betatron tunes to keep the beam away from

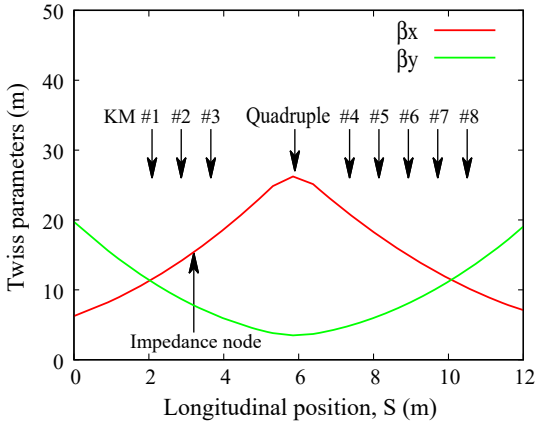

FIG. 9. Twiss parameters (β_x and β_y) in the extraction kicker region. The impedance node in the simulation is placed at the average β_x, as shown by the red arrow.

resonances. A chromatic tune spread is expressed as the product of beam momentum spread ($\Delta p/p$) and lattice ξ. By using the RCS parameters listed in Table I, the chromatic tune spread at injection for the maximum $\Delta p/p$ of 1% is estimated to be as much as 0.1.

Figure 10 shows the calculated horizontal chromaticities (ξ_x) (broken lines) for sextupole (SX) field strength factors as functions of time. An SX strength factor of 1 with an ac field (SX ac) guarantees a full correction ($\xi_x = 0$) throughout the entire acceleration cycle, while no ξ_x correction occurs when SX is turned off (SX off). The SX with a dc field (SX dc) with a strength factor of 1 at the injection energy leads to a full correction of ξ_x only at the injection energy, but the SX field strength decreases gradually as the beam is accelerated, resulting in a decreasing correction of ξ_x and almost no ξ_x correction at the end of the cycle. We call this pattern "SX dc ×1," where "×1" means a full correction of ξ_x at injection. In this study, we also

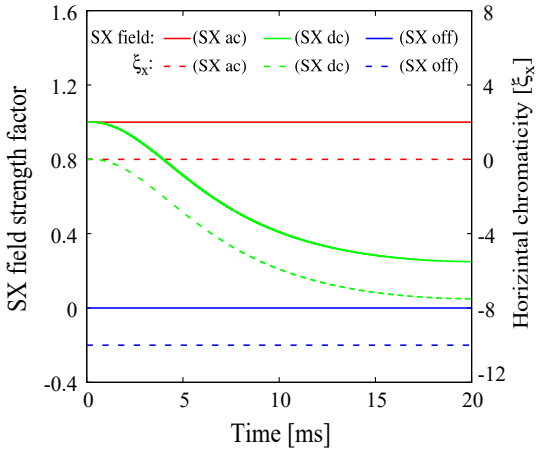

FIG. 10. SX field strength factor and chromaticity ξ_x as functions of the beam acceleration time in the RCS. The situation is the same for ξ_y.

considered reduced SX dc fields, namely, "SX dc ×0.5" and "SX dc ×0.25" for ξ_x correction at the injection energy by a half and by a quarter, respectively. The situation is exactly the same for the vertical chromaticity (ξ_y).

V. BEAM INSTABILITIES: COMPARISON BETWEEN SIMULATED AND MEASURED RESULTS

In this section, we present and compare the details of simulated and measured results of beam instabilities at beam powers up to 0.5 MW, which was the maximum beam power available until 2013. First, we clarify the definition of beam power used throughout this paper. In this study, the beam was delivered either by a single shot on demand or at a lower repetition rate than the designed 25 Hz. The measured number of particles was used to calculate the beam power, based on the 25 Hz "equivalent beam power." We performed systematic studies on the dependence of beam instability growth on various parameters, such as choice of betatron tunes, the momentum spread ($\Delta p/p$) of the injected beam, and the degree of chromaticity correction.

A. Beam instability up to a beam power of 0.5 MW

Until 2013, the output energy of the linac and, thus, the RCS injection energy (E_{inj}) was 0.181 GeV. At the end of 2013, the injection energy was upgraded to the designed 0.4 GeV. The extraction energy was always at the designed value of 3 GeV. Beam instability up to the beam power of 0.5 MW has been studied for both injection energies.

Figure 11 shows the instability results obtained in the simulation for an output beam power of 0.5 MW. The horizontal axis represents the acceleration time, while the vertical axis represents the turn-by-turn horizontal beam position at a beam position monitor (BPM) located in the injection area [39]. The difference between the data in the left and the right plots is the beam energy at injection, which was 0.181 and 0.4 GeV, respectively. The kinetic energies of the beam calculated by using the acceleration pattern are depicted at the top of each figure for 5 ms intervals. The rms $\Delta p/p$ of the injected beam was 0.08%, while a transverse injection painting emittance of 100π mm mrad and the full longitudinal injection painting were applied in both cases. The time-dependent beam position offset at the beginning of the cycle represents the time-dependent closed orbit variation in transverse injection painting, because the BPM was located in the injection area. Ripples in the beam position can be seen clearly, especially for E_{inj} of 0.181 GeV, and they are caused mainly by the 1 kHz switching noise in the power supply (PS) of the main dipole magnets [31]. The 100 kHz ripples caused by the injection dc chicane magnets (SB) persist until 1 ms, during the first half of which they are used for beam injection and they are then turned off during the

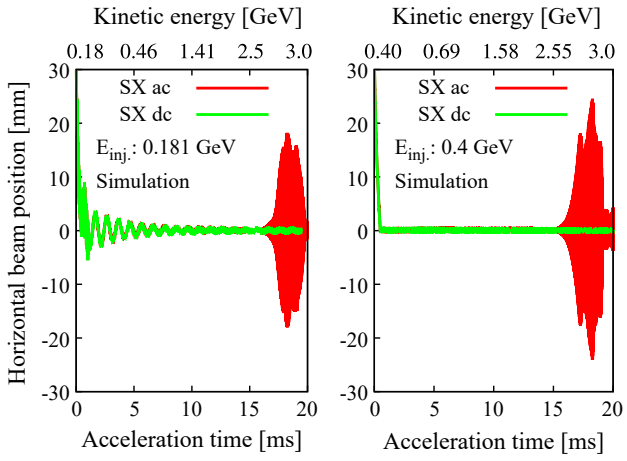

FIG. 11. Beam centroid motion and instability growth due to the transverse impedance of extraction kicker magnets, as obtained in the simulation at a beam power of 0.5 MW. The values of E_{inj} in the left and the right figures are 0.181 and 0.4 GeV, respectively. Beam instability occurs only when ξ is fully corrected for the entire acceleration period, but no beam instability occurs if ξ is fully corrected only at the injection energy.

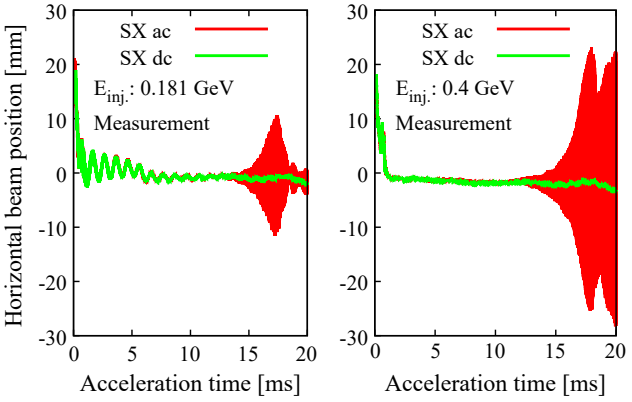

FIG. 12. Measured results of the beam centroid evolution at 0.5 MW beam power. The experimental results agree well with those obtained in the simulations (Fig. 11).

subsequent 0.5 ms [27]. However, the ripples are compensated almost completely when the injection energy is 0.4 GeV. The 1 KHz switching noise was compensated by optimizing the phase and the strength of the orbit correctors (steering magnets) used for correcting closed orbit distortion, while the 100 KHz ripples were eliminated by designing the new PS of the SB to be ripple-free [27]. The corresponding measurement results are shown in Fig. 12. The evolutions of the beam centroid caused by the KM impedance as obtained by the simulated results are found to be in good agreement with the corresponding measured results. The characteristics of beam instability at the beam power of 0.5 MW can be summarized as follows.

Beam instability occurs (red lines in Figs. 11 and 12) only when the ξ is fully corrected to zero for the entire acceleration cycle by using SX ac (red lines in Fig. 10), while no beam instability occurs (green lines in Figs. 11 and 12) when ξ is fully corrected at injection energy only, but the ξ correction is reduced as a function of time by using the SX dc pattern (green lines in Fig. 10). This is a very general behavior of the beam instability growth dependence on ξ; namely, the beam instability is suppressed when the ξ is kept higher.

It has also been observed that the beam instability growth rate is slightly higher and is more unstable for the case of a higher injection energy (0.4 GeV) as compared to the case of a lower injection energy (0.181 GeV). It is possible that this could be caused by suppression of the space charge force at a higher injection energy compared to that at the lower injection energy. The Landau damping effect of the nonlinear space charge force is smaller for the higher injection energy case, resulting in an enhancement of beam instability growth at the higher injection energy, and vice versa for the lower injection energy case. Also, the KM impedance is higher for a relativistic beam, as shown in Fig. 3. The beam instability growth rates obtained by exponential fittings of the experimental data for the 0.181- and 0.4-GeV injections were 759 and 900 s^{-1}, respectively.

The betatron tune shift of the beam centroid caused by the space charge and the transverse horizontal impedance of extraction kicker magnets was calculated from the turn-by-turn beam position data for different beam intensities. Figure 13 shows a comparison of horizontal tune (ν_x) between the simulation (left) and measurement (right) as a function of the beam intensity. The injection and extraction energies were 0.4 and 3 GeV, respectively, while the ξ was fully corrected for the entire acceleration cycle. The horizontal betatron tune ν_x was obtained from a FFT of turn-by-turn simulated and measured beam positions for 1000 turns at around the middle of the acceleration cycle (10 ms). The measurement error for the experimental data

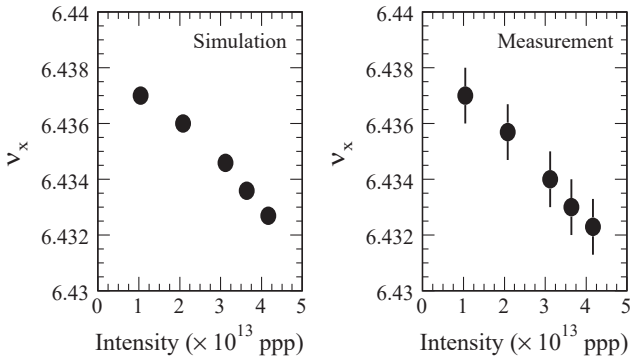

FIG. 13. Simulated (left) and measured (right) results of beam intensity versus tune ν_x, obtained from FFTs of turn-by-turn beam positions for 1000 turns at the middle of the acceleration cycle of 10 ms.

was estimated by $1/N_{\text{turns}}$, where N_{turns} is the number of turns used for the FFT. The bare tune at this time during acceleration was set to be 6.4375 (details given in a later section). The detuning of ν_x at a higher beam intensity is almost linear, while the shifts of ν_x for the maximum beam intensity of 4.16×10^{13} in this study were obtained to be -0.0047 and -0.0052 in the simulation and measurement, respectively. It is important to mention that no beam instability occurs at beam intensities up to 2.1×10^{13}.

B. Beam instability suppression by space charge

The above arguments for beam instability suppression can be directly checked for the condition when the effect of space charge on the beam is considerably higher than that presented in Figs. 11 and 12. For that purpose, we compare results, both simulated and measured, for two cases: (i) include only the fundamental rf voltage (V_1), turn off the second harmonic rf voltage (V_2), and do not apply longitudinal injection painting; (ii) include dual harmonic rf voltages and also apply longitudinal injection painting. These alternative injection scenarios will lead to a higher peak space charge density in case (i) than in case (ii). Moreover, we consider the lower injection energy of 0.181 GeV and a beam power of 0.375 MW. All parameters in this case are exactly the same as those shown in Fig. 7, except that chromaticity is fully corrected throughout the acceleration time and the KM impedances are now included in the present simulation.

Figure 14 shows a comparison of such a simulation with measured results in the left and right plots, respectively. The ξ was corrected to be zero for the entire acceleration time in all cases. Beam instability growth occurs (red) in case (ii), when longitudinal injection painting is performed by using dual harmonic rf voltages ($V_1 + V_2$), but it is completely suppressed (green) for case (i), where the space charge force is enhanced by the application of only the fundamental rf voltage (V_1) and by the omission of longitudinal injection painting. The B_f at the end of injection with the application of V_1 alone is 0.27, which is nearly twice as peaked (0.45) as with the application of both V_1 and V_2. The Landau damping effect is more enhanced in the former case, which results in a suppression of beam instability growth. The simulation and the measurement results are very consistent with each other.

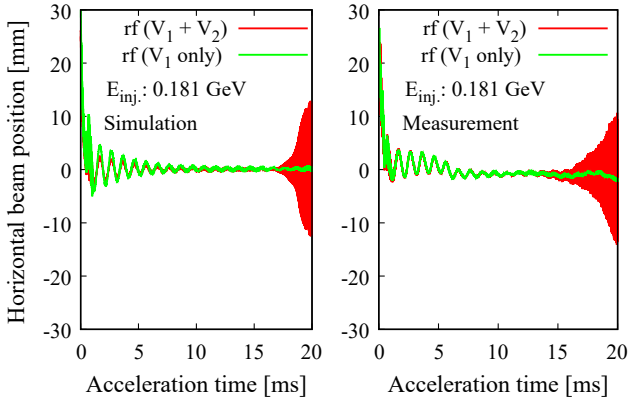

FIG. 14. Simulated (left) and measured (right) results of beam instability suppression by the effect of strong space charge (peaky bunch) for 0.375 MW beam power. The beam tends to be stable (green) when the space charge effect is strengthened by turning off the second harmonic rf voltage (apply V_1 only) and by not performing longitudinal injection painting.

We have also found that, in this particular condition with strong space charge, the stability has no significant dependence on the transverse injection painting emittances. Figure 15 shows simulation results of the dependence of beam centroid evolution on transverse injection painting emittances from 50π mm mrad up to a maximum available of 200π mm mrad for a beam power of 0.375 MW. The plot in green corresponds to that shown by the same color in Fig. 14. The Landau damping effect is quite significant in the presence of strong space charge for any transverse beam emittances considered in the present study.

However, it should be noted that in a condition when instability occurs the beam instability growth rate has a dependence on the choice of transverse emittance, but the impact is small on the stabilization of the beam. On the other hand, we found that the size of the vacuum chamber, by which the indirect space charge effect is changed, plays an important role for stabilization of the beam. In the above condition by using only the fundamental rf voltage, we have studied the effect of indirect space change by changing the radius of the conducting wall, which is used as a boundary condition for the space charge calculation. The details of the simulation results of the beam instability dependence on the radii of the vacuum chamber are given in the rest of the present subsection.

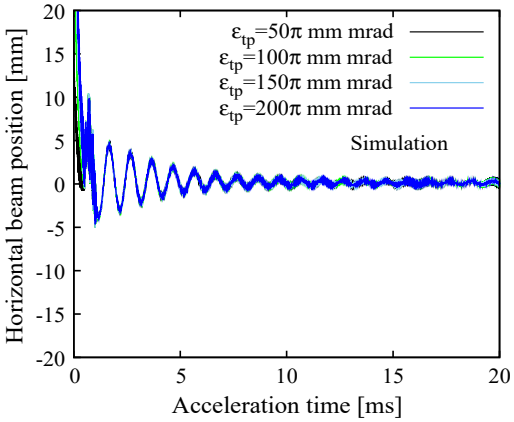

FIG. 15. Simulation results of beam instability growth dependence on the transverse injection painting emittances for 0.375 MW beam power and applying only V_1. In this particular condition with strong space charge effect, the Landau damping effect is quite significant, resulting in no remarkable difference on the beam stability condition within the present variation of transverse beam emittance.

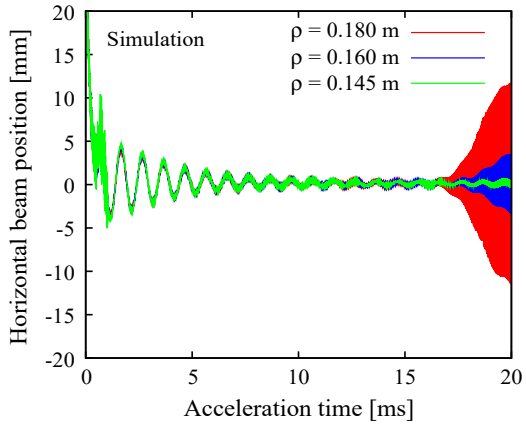

FIG. 16. Simulation results of beam instability growth dependence on the vacuum chamber radius ρ. The indirect space charge effect is reduced by an increase of ρ, and the beam tends to destabilize with increasing ρ.

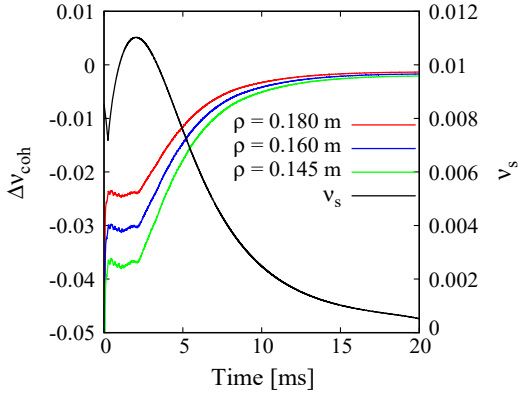

FIG. 17. Estimated $\Delta\nu_{coh}$ as a function of time for three different vacuum chamber radii for a beam power of 0.375 MW. The synchrotron tune ν_s is also shown by the black line. The injection and extraction energies are 0.181 and 3 GeV, respectively.

Next, we studied the dependence of the beam instability growth rate on the indirect space charge effect parametrized by the radius of the vacuum chamber ρ. Figure 16 shows simulation results of the beam centroid evolution dependence on ρ. The actual value of ρ in the RCS is 0.145 m (green), but it was enlarged to 0.160 (blue) and 0.18 m (red) for the present study. The plot in green is the same as those shown by the same color in Figs. 14 and 15. The beam tends to be unstable even if ρ is enlarged by just 10% (blue), and it becomes further destabilized as ρ is further increased. The coherent tune shift, as given by $\Delta\nu_{coh}$, is reduced as ρ is increased, and the beam tends to be more unstable. It is worth mentioning that the effect of space charge at a lower energy due to a change of ρ has also been observed in terms of beam losses. In contrast to the beam instability growth rate, the beam survival rate is improved with respect to an increase of the ρ. This is mainly due to the reduction of the destabilizing image forces as ρ is increased. The number of particles at $\nu_{x,y} = 6$ is reduced (see Fig. 8, top left side) due to $\Delta\nu_{coh}$ is reduced as ρ is increased. However, the Landau damping effect vanishes earlier, resulting in a higher beam instability growth rate as ρ is enlarged.

Figure 17 shows an estimated $\Delta\nu_{coh}$ over the entire acceleration cycle using Eq. (2) for the three above values of ρ. The beam parameters are the same as those listed at the top of Table III, except that the rf voltage was taken to be only the fundamental harmonic in this case (the same as Figs. 14–16). As a result, the bunching factor at the injection energy becomes smaller, $B_f = 0.27$, but it is almost the same, $B_f = 0.16$, at the extraction energy. The synchrotron tune ν_s as a function of acceleration time is also shown by the black line. The value of $\Delta\nu_{coh}$ compared to ν_s is about a factor of 3 higher at a lower energy and gradually approaches the absolute value of ν_s as the beam energy increases. However, it never becomes less than ν_s as long as ρ is smaller than 0.180 m. If one considers the dependence of the beam instability growth rate on the relative difference between these two parameters, the present study reveals that a higher ratio of $\Delta\nu_{coh}$ to ν_s results in a more stable beam within the parameter range studied in this work.

Figure 18 shows simulation results of coherent horizontal betatron tune spectra for the three radii ρ. The tune shift is inversely proportional to the square of ρ according to Eq. (2). The frequency spectra were obtained from FFTs of a turn-by-turn beam centroid for 2000 turns at around 15 ms and subtracted from the bare tune in order to obtain the tune shift $\Delta\nu_x$. The simulation conditions are exactly the same as in Fig. 16, except KM impedance was not taken into account. The indirect space charge effect is increased with increasing ρ, resulting in the peak in ν_x approaching the bare tune. However, the beam tends to be more unstable as ρ is increased.

In the simulation, we have also calculated the rms spread of the betatron tune at different times of acceleration including near the beam instability onset at about 15 ms. Table IV shows a rms spread of the horizontal betatron tune

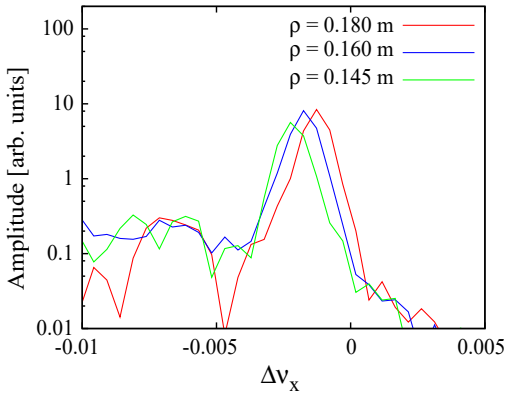

FIG. 18. Simulation results of betatron frequency spectra for choices of the vacuum chamber radius, representing a horizontal betatron tune shift at around 14 ms of the acceleration time.

TABLE IV. Calculated rms spread of horizontal betatron tune $\sigma_{\nu x}$ by changing the radius of the vacuum chamber. The tune spread is reduced as ρ is increased, but the beam tends to be more unstable with an increasing ρ (Fig. 16).

Acceleration time [ms]	$\sigma_{\nu x}$ ($\rho = 0.145$ m)	$\sigma_{\nu x}$ ($\rho = 0.180$ m)
7.0	0.063 88	0.062 10
12.0	0.030 46	0.028 88
15.0	0.023 52	0.023 21

($\sigma_{\nu x}$) for the two cases of vacuum chamber radius ρ of 0.145 and 0.180 m. The tune spread is also obtained to be reduced as ρ is increased, but the beam becomes more unstable as ρ is increased.

From the above simulation studies, it appears that the indirect space charge effect due to the vacuum chamber plays an important role for the stabilization of the beam. The chamber radius has a strong impact on the stability rather than the transverse emittance of the beam.

VI. BEAM INSTABILITY BEYOND 0.5 MW BEAM POWER AND STRATEGY FOR ACCOMPLISHING 1 MW

To accomplish the designed 1 MW beam power, the peak current of the H^- beam in the linac was upgraded from 30 mA to the designed 50 mA in 2014. By this time, we had conducted detailed systematic simulation studies on the beam instability scenarios beyond 0.5 MW beam power to prepare realistic guidelines for accomplishing the designed beam power of 1 MW. This is one of the main goals of the present study. Although no beam instability occurs up to beam powers of 0.5 MW when chromaticity ξ is fully corrected only at the injection energy by a SX dc field, the simulation results yielded very sensitive beam instability scenarios for beam powers higher than 0.5 MW. With a full dc chromaticity correction, the beam exceeds the instability threshold even at a beam power of 0.75 MW. Based on the detailed simulation studies, the following strategies were formulated to stabilize the beam at 1 MW: (i) careful manipulation of the horizontal betatron tune (ν_x) during the acceleration cycle, (ii) selection of narrower $\Delta p/p$ of the injected beam, and (iii) further reduction of SX dc fields to reduce the degree of chromaticity ξ correction throughout the acceleration cycle.

Figure 19 shows six typical horizontal betatron tune (ν_x) manipulations from injection until extraction including one case (a) without any manipulation, as considered in the simulation studies. The choice to manipulate ν_x is very important, because the transverse horizontal impedance of the RCS extraction KMs excites only the transverse horizontal beam instability. The ν_x without any manipulation corresponds to the top most line denoted by (a), while (b)–(g) are manipulated as functions of time by using between two and five of the seven quadrupole magnet families. The tune ν_x at injection is typically set to 6.45, but it must be lowered to at least 6.40 by the end of the cycle. The vertical tune (ν_y), is typically set to 6.42 at injection.

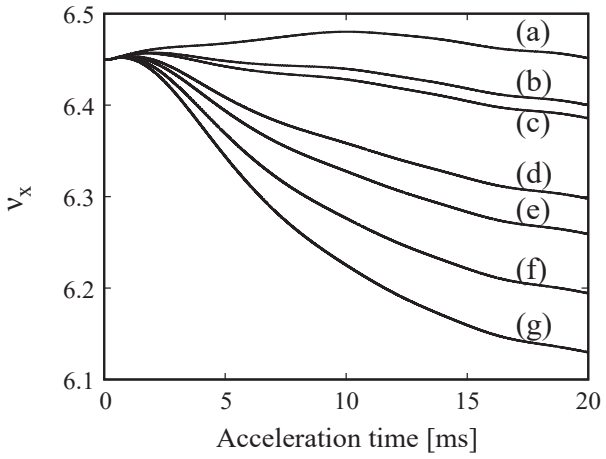

FIG. 19. Manipulation of tune ν_x to suppress beam instability at beam power of 1 MW. The ν_x at injection is typically set to 6.45, but it has to be manipulated as a function of time in order to stabilize the beam. The ν_x without any manipulation corresponds to the line denoted by (a).

The ν_x and ν_y setting of 6.45 and 6.42, respectively, at injection energy is important for beam loss mitigation, but ν_x, in particular, must be manipulated carefully as a function of time to avoid beam instability, which appears later in the acceleration cycle. The tracking errors between the bending and the quadrupole magnets lead to a temporal variation of ν_x even without any manipulation, as shown by Fig. 19(a).

The manipulation of ν_x, as shown in Fig. 19, was needed at beam powers exceeding 0.7 MW. Figure 20 shows a comparison of the simulated (top) and the measured (bottom) results for the beam power of 0.75 MW. The injected $\Delta p/p$ in this case was 0.18% (rms), while the SX dc pattern was applied for ξ fully corrected only at the injection energy. The ν_x manipulation pattern denoted by Fig. 19(b) was applied in this study. The measurement results were found to be very consistent with the corresponding simulation, and the proposed manipulation of ν_x to stabilize the beam was demonstrated successfully. Detailed studies with all given tune manipulations were done for 1 MW beam power and will be described in the next section.

In a further experiment, the advantage of using a narrower $\Delta p/p$ in the injected beam for suppressing beam instability was also confirmed. Figure 21 shows a comparison between the simulation (green) and the measurement (blue) results with no tune manipulation, when the rms injected $\Delta p/p$ was set to 0.08% instead of 0.18%, as in the above case (Fig. 20). Unlike previous results, the selection of a narrower $\Delta p/p$ in the injected beam stabilizes the beam even with no tune manipulation. This is an alternate way to suppress the beam instability. These results also demonstrate the effect of space charge on the beam instability, which in this case one may think about the

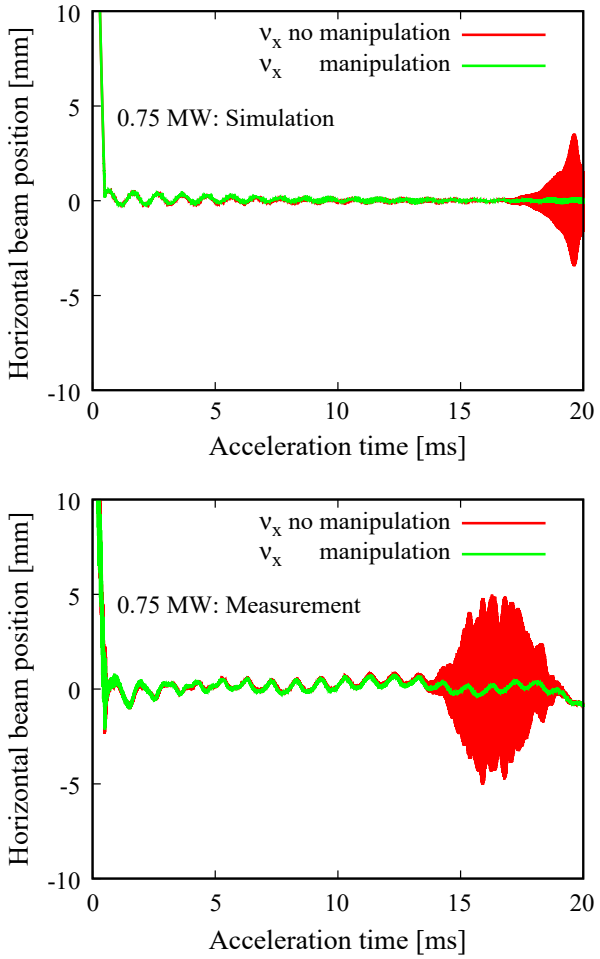

FIG. 20. Simulated (top) and measured (bottom) results of beam instability growth at a beam power of 0.75 MW. The beam instability, which occurs without any tune manipulation, can be well mitigated by applying a proper tune manipulation.

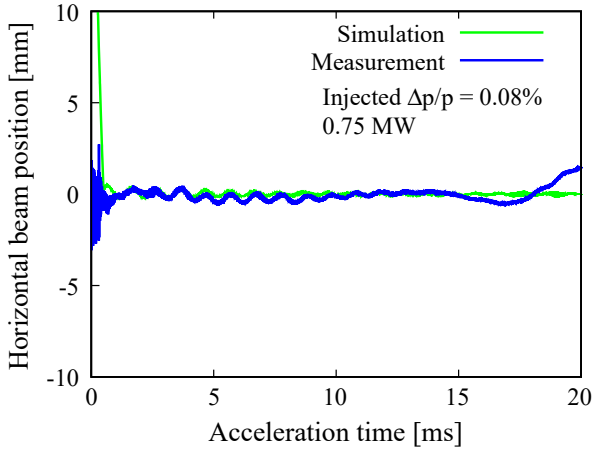

FIG. 21. Demonstration of beam instability suppression in the simulation (green) as well as in measurement (blue) by using a narrower momentum spread $\Delta p/p = 0.08\%$ (rms) in the injected beam.

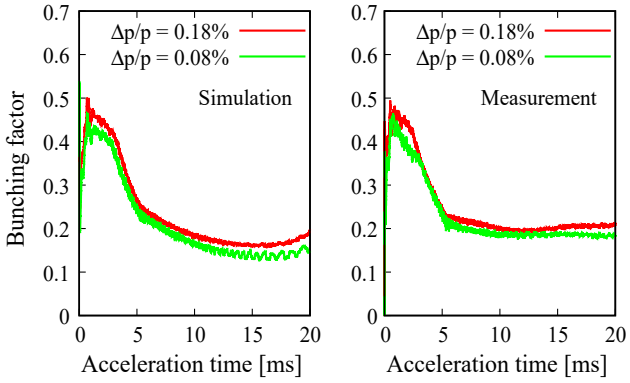

FIG. 22. Simulated (left) and measured (right) results of bunching factor B_f with rms injected $\Delta p/p$ of 0.18% and 0.08% as shown by the red and green lines, respectively.

change of the incoherent betatron tune spread of the circulating beam due to a change of $\Delta p/p$ of the injected beam. In the previous study presented in Fig. 14, the rf voltage patterns were changed to obtain stability. However, in this study, standard dual harmonic rf patterns including longitudinal injection painting parameters were maintained, and only the $\Delta p/p$ in the injected beam was changed. A narrower $\Delta p/p$ in the injected beam produces a narrower (peaky) longitudinal phase space distribution in the RCS, resulting in a stronger space charge bunching as compared to that achieved with a wider $\Delta p/p$. The Landau damping is more effective for suppressing beam instability in the case of a more strongly bunched beam with higher peak space charge forces.

Figure 22 shows the calculated (left) and measured (right) bunching factors (B_f) obtained for a beam power of 0.75 MW. The rms $\Delta p/p$ of the injected beam was 0.18% and 0.08% for the plots in red and green lines, respectively. The effect of space charge is comparatively higher when the B_f is lower, which is obtained by using a narrower $\Delta p/p$ in the injected beam, and the beam tends to be stable in such a case.

However, in contrast to its effect on the beam instability, a wider $\Delta p/p$ (0.18%) in the injected beam is more suitable for reducing the space charge effect at lower energies to mitigate the beam loss at 1 MW. Although a beam instability up to 0.75 MW (Fig. 20) can be well suppressed by proper tune manipulation with ξ fully corrected only at the injection energy by SX dc, the beam at 1 MW is unstable for any tune manipulation even if the ξ is corrected only at the injection energy. As a result, a further reduction of the SX dc fields for reducing the degree of ξ correction must be implemented for complete suppression of beam instability at 1 MW.

VII. ACCOMPLISHMENT OF DESIGNED 1 MW BEAM POWER

To accomplish the designed 1 MW beam power, we applied a further reduction of the degree of chromaticity (ξ)

TABLE V. The degree of SX dc field strength factor versus horizontal (ξ_x) and vertical (ξ_y) chromaticities at the injection and extraction energies. The "SX dc ×1" here is same as the "SX dc" shown in Fig. 10 and stated throughout the text.

SX strength factor	ξ_x, ξ_y (at injection)	ξ_x, ξ_y (at extraction)
dc ×1	0, 0	−7.5, −5.3
dc ×0.5	−5, −3.5	−8.8, −6.1
dc ×0.25	−7.5, −5.3	−9.4, −6.6
Off	−10, −7	−10, −7

correction in addition to careful tune manipulation. This is because the beam instability growth rate can be suppressed by ensuring that the ξ of the machine is close as possible to the natural value [11]. Table V shows a comparison of the degree of SX dc field strength versus ξ at the injection and extraction energies. SX off ensures no correction of ξ, thus guaranteeing the natural ξ for the entire energy range.

Figure 23 shows a comparison of simulated and measured results for beam instability dependence on the horizontal betatron tune (ν_x) manipulations (b)–(g) (in Fig. 19), when ξ_x and ξ_y were corrected only a quarter of full at injection with almost no correction at extraction by applying SX with dc ×0.25 pattern as shown in Table V. As shown in Fig. 20, a manipulation of ν_x was necessary for beam instability suppression beyond 0.75 MW beam power, but the scenario at 1 MW is even more difficult. The choice of ν_x manipulation is very limited even when almost no chromaticity correction is applied. The beam instability occurs for all ν_x manipulations, except for only two patterns, (b) and (e). The simulated results of characteristic dependence of the beam instability growth rate on the betatron tune and its suppression by using a proper manipulation of the betatron tune was found to be consistent with the corresponding measured results.

In addition to beam instability suppression, the choice of tune manipulation has to be considered to keep the transverse emittances of the extracted beam as low as possible. This is because, due to large space charge detuning at a lower energy, a portion of the transverse beam crosses various low-order nonlinear systematic resonances, resulting in higher emittance dilutions. The effect is comparatively larger in the vertical plane, as the bare tune ν_y at injection was set lower (6.42) than that of ν_x (6.45). For the details of beam dynamics, the following beam instability studies at 1 MW were carried out using the tune manipulation pattern denoted by Fig. 19(b). In the simulations and in the subsequent measurements, we have confirmed that (b) is the only suitable ν_x manipulation pattern to satisfy RCS operation at the designed beam power of 1 MW.

Figure 24 shows detailed simulation results of the beam instability suppression at 1 MW by controlling the degree of ξ correction through the SX dc fields. The ν_x manipulation (b) shown in Fig. 19 is applied. The plot in red corresponds to a SX dc field with a strength factor 1 at injection (SX dc ×1) for full ξ correction at the injection

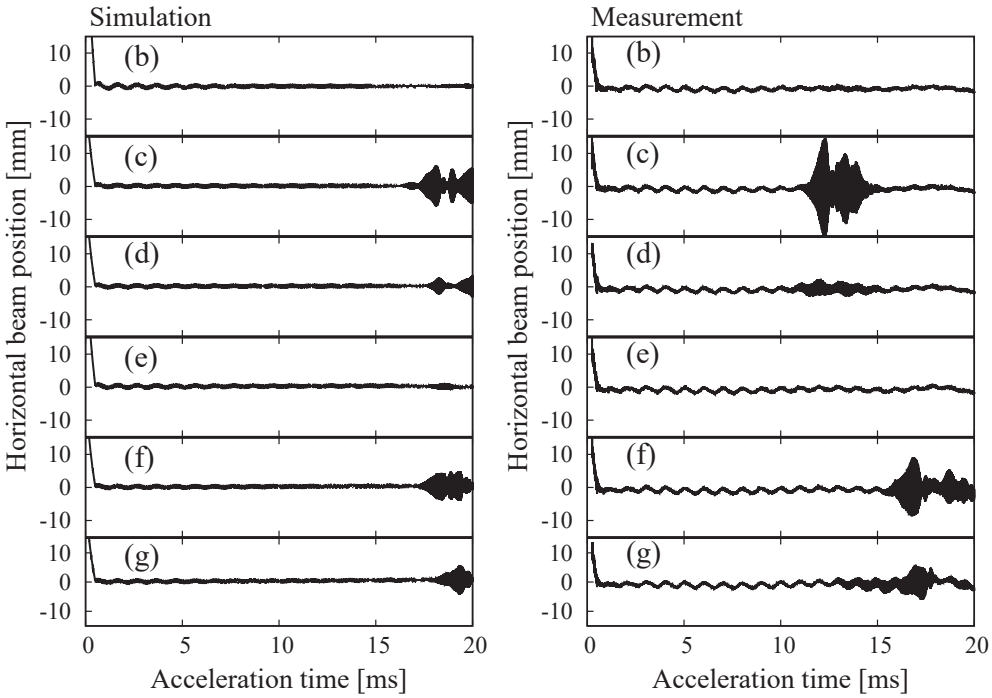

FIG. 23. Simulated (left) and measured (right) results of beam instability dependence on ν_x manipulations [Figs. 19(b)–19(g)], for 1 MW beam power, when only a quarter of the full chromaticity correction at injection by using dc ×0.25 field was applied. With a very severe beam instability at 1 MW, the simulation results show the necessity of a proper choice of ν_x manipulations in order to suppress the beam instability. Simulated and experimental results were found to be consistent in all cases.

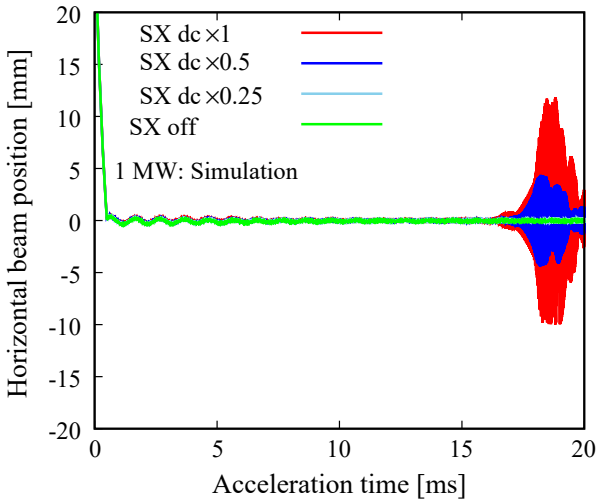

FIG. 24. Simulated results of beam instability suppression at 1 MW obtained by reducing the degree of chromaticity correction. In addition to the proper manipulation of ν_x (see Fig. 19), no more than a quarter of the full ξ correction at injection and almost no correction at extraction can be applied to stabilize the designed beam power of 1 MW.

energy only (green solid and dashed lines in Fig. 10 for the SX field and ξ_x, respectively). The plots in other colors correspond to a reduction of the degree of ξ correction to half and quarter at injection by further scaling down the SX dc ×1 field to SX dc ×0.5 (blue) and SX dc ×0.25 (sky blue). The green curve shows a case where no ξ correction was applied (blue dotted line in Fig. 10) by turning off SX for the entire cycle. The beam is unstable even when the degree of ξ correction is reduced by half at injection.

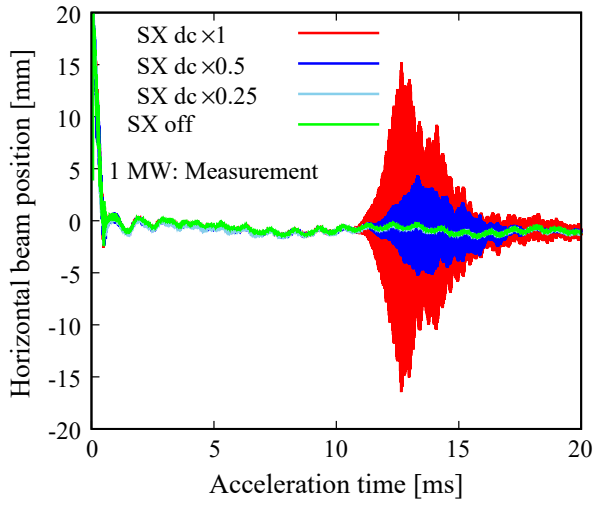

FIG. 25. Measured beam instability mitigation at a beam power of 1 MW by reducing the degree of chromaticity correction using the same patterns as those applied in the simulations (Fig. 24). Similar to the simulation results, the designed 1 MW beam acceleration was accomplished by keeping ξ as close as possible to the natural value with SX dc ×0.25 or SX off.

A further reduction of ξ correction is thus necessary for the complete suppression of beam instability. A quarter of full ξ correction at injection (SX dc ×0.25) or no ξ correction (SX off) leads to the complete suppression of beam instability at 1 MW. The simulation results thus mean that ξ must be as close as possible to the natural value over the entire cycle to accomplish the designed 1 MW beam power.

Figure 25 shows the corresponding measurement results at 1 MW beam power. The measured beam instability results at 1 MW were found to be consistent with the simulation results in all cases. Beam instability growth tends to decrease significantly with higher ξ in the machine, and beam instability is eliminated by reducing the ξ correction to at most a quarter at injection (SX dc ×0.25), as compared to that with a full correction at injection (dc ×1). A combination of a proper betatron tune manipulation (Fig. 19) and minimal ξ correction were used to accomplish the designed 1 MW beam by successfully mitigating the beam instability caused by transverse impedance of the extraction kicker magnets [2].

VIII. LIMITATION OF PARAMETER SPACE DUE TO KICKER IMPEDANCE

Based on detailed systematic simulation and experimental studies, we have just barely been able to mitigate the beam instability caused by the huge impedance of the RCS extraction KMs and accomplish the designed 1 MW beam power. However, it has already been understood that such a huge impedance puts a strong limitation on the beam and machine parameters, such as the momentum spread ($\Delta p/p$) of the injected beam, the betatron tunes, and the degree of chromaticity (ξ) correction. The RCS is a multiuser machine, and it operates simultaneously for the MLF and MR. These two facilities have diverse and differing requests in terms of beam parameters, including beam intensity [1,36]. However, many parameters cannot be changed simultaneously between pulses in the RCS. To stabilize the beam power at 1 MW, the minimal or zero ξ correction scheme must be applied at this stage in the beam study. However, at the injection energy of 0.4 GeV, the ξ correction minimizes the betatron tune spread and the corresponding transverse beam emittances. Lower emittance of the beam extracted from the RCS is beneficial for downstream facilities, especially for the MR, from the viewpoint of reducing beam losses at the beam transport from the RCS to the MR, as well as within the MR. For example, at the present RCS operation, the transverse injection painting emittance for the MR beam is kept as low as possible (50π mm mrad) in order to achieve a lower emittance of the extracted beam, while it is as high as 200π mm mrad for the MLF beam.

Figure 26 shows the simulated transverse rms emittances (ϵ_{rms}) at the extraction energy as a function of the SX dc field strength factors (four patterns including SX off, as shown in Figs. 24 and 25). The KM impedance is not

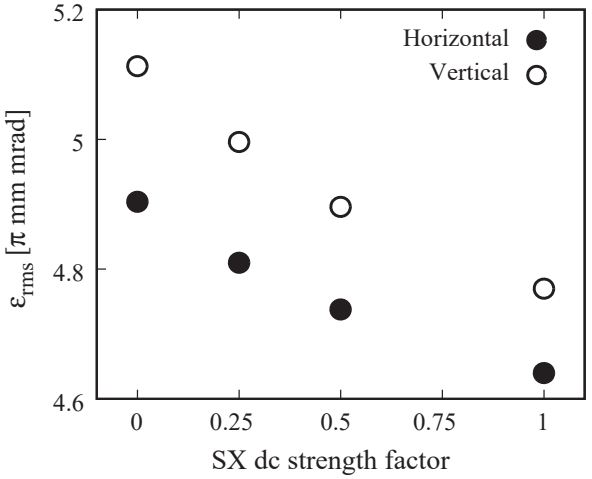

FIG. 26. Transverse ϵ_{rms} of the circulating beam at the extraction energy obtained in the simulation as a function of the degree of chromaticity correction controlled by a SX dc field. Disregarding KM impedances, which are not included in these results, fully corrected ξ at the injection energy leads to the minimum beam emittances extracted from the RCS.

considered in the present simulation. A higher degree of ξ correction at injection leads to lower transverse beam emittances, where the minimum value of ϵ_{rms} was obtained by applying a full ξ correction at the injection energy by using the SX dc ×1 pattern (green lines in Fig. 10). However, beam instability excited by a KM impedance leads to the worst case when ξ is corrected only at the injection energy by using a SX dc ×1 field (see Figs. 24 and 25), and that limits the degree of ξ correction. Other than the limitation on the degree of ξ correction, there is almost no choice in terms of the betatron tune. The proposed tune manipulation pattern (Fig. 19) leads to the minimum beam instability growth rate among all available patterns. It is worth mentioning that, with slightly different experimental conditions, a similar dependence of the transverse beam emittances on the degree of ξ correction has been measured recently at around 6 ms of the acceleration process [40]. Therefore, reducing the KM impedance is also essential for improving the quality of the beam extracted from the RCS.

Other than beam quality, there is another reason why reducing KM impedance is a must. The MR operation cycle for fast extraction will be upgraded from the present 2.48 s to about 1 s in the near future [41]. As a result, the RCS beam sharing ratio between MLF and MR will be changed from 0.94:0.06 to 0.84:0.16. This is because, in the new scheme, four out of 25 pulses in the RCS (25 Hz) will be delivered to MR in each second, while the remaining 21 pulses will be delivered to MLF. To make sure that the designed 1 MW beam power delivery to the MLF is achieved, one instantaneous pulse to the MLF should be equivalent to a beam power of 1.2 MW. The corresponding number of particles per pulse in the MLF beam should be 9.996×10^{13} instead of 8.33×10^{13}. We have to ensure that no beam instability occurs at least up to that beam intensity in the RCS.

In addition, the construction of a second target station in the MLF has been planned. Although a detailed beam sharing scenario has not been fixed yet, it will require an increase in the RCS beam power. A midterm plan for the RCS beam power upgrade has been set to 1.5 MW (1.25×10^{14} ppp) to accommodate the above changes in the RCS beam sharing in the near future. However, beam instability beyond 1 MW occurs even with no ξ correction over the entire cycle, and this is at present the most significant issue from the viewpoint of exceeding the designed 1 MW beam power in the RCS.

IX. BEAM INSTABILITY SUPPRESSION BY REDUCING THE KM IMPEDANCES

To achieve an adequate variation in the choice of the parameter space at 1 MW operation and to realize beam powers beyond 1 MW, the reduction of KM impedances is very important. We have studied the extent to which KM impedances are tolerable to meet those requirements. Recently, a direct measure to suppress KM impedances has been proposed and demonstrated experimentally [5,10]. The idea is to insert diodes and matched resistors between the pulse forming line of the KM power supplies and the coaxial cables in order to dump the beam-induced voltage by circulating a beam during its passage through the KMs. The method could demonstrably reduce KM impedance to at least half that without any further measures.

We have considered the newly given reduced impedance in simulations to check its effectiveness on the beam

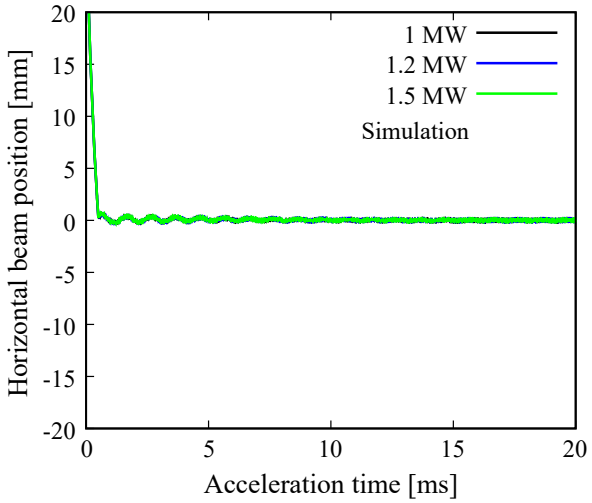

FIG. 27. Simulated results of beam centroid growth for beam powers of 1 (black line), 1.2 (blue line), and 1.5 MW (green line) employing reduced KM impedances by nearly a half. Beam powers beyond 1 MW can also be stabilized even with fully corrected ξ at the injection energy by using the SX dc ×1 field.

instability suppression. Figure 27 shows the simulation results for beam powers of 1, 1.2, and 1.5 MW denoted by the black, blue, and green colors, respectively. The ξ is fully corrected for the injection energy by using the SX dc $\times 1$ field in all cases. As can be seen in the figure, by halving the KM impedance compared to its present value, the beam can be stabilized for beam powers up to 1.5 MW even when applying a full ξ correction at the injection energy. For comparison, the beam instability growth rate using the present KM impedance for a beam power of 1 MW can be seen in Fig. 24, plotted in red.

The present results also mean that the RCS can achieve more than the designed 1 MW of beam power if the present KM impedances are reduced by half and the system is capable of performing beam extraction. The present simulation results recently increased the motivation for detailed R&D studies on realistic measures for reducing KM impedances, including ensuring that the system performs beam extraction without any problem.

X. SUMMARY

The transverse impedance of the extraction KMs is a significant source of beam instability that presents a big hurdle from the viewpoint of realizing the designed 1 MW beam power in the 3-GeV RCS at Japan Proton Accelerator Research Complex. To study the coupled bunch beam instabilities excited by the KM impedance and to determine measures to suppress the beam instability, realistic beam simulations considering including space charge were carried out by using the ORBIT particle tracking code. The code was first made capable of taking into account all realistic time-dependent machine parameters, error sources, and transverse and longitudinal injection painting processes. The space charge simulation results have been confirmed to be very consistent with corresponding measurement results. Then we have also upgraded the impedance model in the ORBIT code to incorporate realistic time-dependent impedances for the beam instability simulations.

The beam instability up to a beam power of 0.5 MW occurs only when the chromaticity is fully corrected over the entire acceleration cycle, while no beam instability occurs if chromaticity is fully corrected only at the injection energy. The effect of space charge on beam instability suppression has been observed in various simulations and the corresponding measurements. In the present study, it appears that the indirect space charge effect due to the vacuum chamber plays an important role for the stabilization of the beam. The chamber radius has a strong impact on the stability rather than the transverse emittance of the beam.

The beam instability picture at the designed beam power of 1 MW is found to be more severe and constraining in the simulation results. In contrast to the beam instability at a beam power up to 0.5 MW, a strong beam instability occurs even if chromaticity is fully corrected at the injection energy. The realistic strategies obtained by systematic simulation studies include the proper manipulation of the betatron tune and a further reduction of the degree of chromaticity correction even at the injection energy. Namely, chromaticity can be corrected moderately at lower energies, but it should be kept close to the natural value at higher energies. A correction of chromaticity to a quarter or lower at the injection energy and almost no chromaticity correction at the extraction energy is needed to stabilize the beam at 1 MW. The details of the beam instabilities obtained in the simulations are reproduced well in the measurements, and an acceleration of the 1 MW beam has been experimentally accomplished.

However, the large impedance of the KMs strongly restricts the choice of parameters for the operation of the RCS. There exist almost no alternative choices of betatron tune manipulations from the one proposed here. The full correction of chromaticity at the injection energy leads to lower extracted beam emittances but cannot be applied, because strong beam instability occurs at higher energies in such a case. The reduction of KM impedance is therefore very desirable to ensure adequate parameter variation for RCS operation.

We have carried out simulation studies of beam instability scenarios and the associated measures for beam powers up to 1.5 MW, which is the midterm beam power upgrade target for the RCS in order to cope with upgrades in the downstream facilities. In further simulations, we used the newly given KM impedance, which is nearly half of the present KM impedance, as demonstrated to be reduced by appropriate measures. Although beam instability beyond 1 MW occurs with the present KM impedance even if no chromaticity correction is applied, it can be stabilized successfully up to beam powers of 1.5 MW by applying a full chromaticity correction at the injection energy when KM impedance is halved. It is thus very important that the RCS can achieve beam powers exceeding the designed 1 MW, but the reduction of the present KM impedance by at least half is necessary to achieve such beam powers.

In the present study, collective beam dynamics with coupled bunch instabilities in the presence of huge transverse impedances in a megawatt-class multiuser proton machine was performed systematically. We have proposed realistic measures to suppress beam instabilities for accomplishing the designed beam power of 1 MW, to realize up to 1.5 MW of beam power, and also to achieve lower extracted beam emittances, as required by the downstream facilities. The present form of the ORBIT code is fully machine independent and can be implemented successfully on any existing or proposed high-intensity hadron machines for realistic collective beam dynamics simulations considering beam instabilities.

ACKNOWLEDGMENTS

The authors highly acknowledge all members of the J-PARC RCS for their generous support and encouragement

on the present study. We are grateful to Prof. Y. Irie of KEK for many fruitful discussions on the present work. It is also our opportunity to acknowledge Dr. A. Shishlo and Dr. S. Cousineau of Spallation Neutron Source for their valuable supports in the initial stage of ORBIT code implementation for the RCS beam simulations. The authors are also indebted to all staffs of the JAEA large-scale parallel computer system for their cooperation and generous support to use the system, especially in the beginning of the ORBIT code implementation for the RCS beam simulations.

[1] JAERI Technical Report No. 2003-044 and KEK Report No. 2002-13.
[2] H. Hotchi, Recent progress of J-PARC RCS beam commissioning — Toward realizing the 1-MW output beam power, in *Proceedings of the 2015 International Particle Accelerator Conference, IPAC'15, Richmond, VA, USA* (JACoW, Richmond, 2015), p. 1346.
[3] Y. H. Chin *et al.*, Impedance generated by a ceramic chamber with rf shields and TIN coating, in *Proceedings of the 39th ICFA Advanced Beam Dynamics Workshop, HB2006, Tsukuba, Japan* (JACoW, Tsukuba, 2006), p. 125.
[4] Y. Shobuda, Analytical evaluations of coupling impedances of resistive and magnetic bellows, Nucl. Instrum. Methods Phys. Res., Sect. A **741**, 177 (2014).
[5] Y. Shobuda, Y. Irie, T. Toyama, J. Kamiya, and M. Watanabe, Measurement scheme of kicker impedances via beam-induced voltages of coaxial cables, Nucl. Instrum. Methods Phys. Res., Sect. A **713**, 52 (2013).
[6] H. Hahn, BNL/SNS Technical Note No. 135, Brookhaven National Laboratory, 2004.
[7] M. Kinsho, Y. Saito, Z. Kabeya, K. Tajiri, T. Nakamura, K. Abe, T. Nagayama, D. Nishizawa, and N. Ogiwara, Development of alumina ceramics vacuum duct for the 3 GeV-RCS of the J-PARC project, Vacuum **73**, 187 (2004).
[8] M. Kinsho, Y. Saito, Z. Kabeya, and N. Ogiwara, Titanium flanged alumina ceramics vacuum duct with low impedance, Vacuum **81**, 808 (2007).
[9] R. L. Gluckstern, CERN Report No. 2000-011, 2000.
[10] Y. Shobuda *et al.*, in *Proceedings of the 4th International Particle Accelerator Conference, IPAC-2013, Shanghai, China, 2013* (JACoW, Shanghai, China, 2013), p. 1742.
[11] F. Sacherer, CERN Report No. 77-13, 1977, pp. 198–218.
[12] M. Blaskiewicz, Transverse stability with nonlinear space charge, Phys. Rev. ST Accel. Beams **4**, 044202 (2001).
[13] M. Blaskiewicz, Electron cloud instabilities in the Proton Storage Ring and Spallation Neutron Source, Phys. Rev. ST Accel. Beams **6**, 014203 (2003).
[14] A. Burov, Head-tail modes for strong space charge, Phys. Rev. ST Accel. Beams **12**, 044202 (2009).
[15] V. Balbekov, Transverse modes of a bunched beam with space charge dominated impedance, Phys. Rev. ST Accel. Beams **12**, 124402 (2009).
[16] Y. Shobuda *et al.*, in *Proceedings of the 2nd International Particle Accelerator Conference, San Sebastián, Spain* (EPS-AG, Spain, 2011), p. 595.
[17] Y. H. Chin, A. W. Chao, and M. M. Blaskiewicz, Two particle model for studying the effect of space-charge force on strong head-tail instabilities, Phys. Rev. ST Accel. Beams **19**, 014201 (2016).
[18] Y. Shobuda *et al.*, Theoretical elucidation of space charge effects on the coupled-bunch instability at the 3-GeV rapid cycling synchrotron at the Japan Proton Accelerator Research Complex, Prog. Theor. Exp. Phys. (**2017**) 013G01.
[19] V. Balbekov, Threshold of transverse mode coupling instability with arbitrary space charge, Phys. Rev. Accel. Beams **20**, 114401 (2017).
[20] J. A. Holmes, S. Cousineau, V. Danilov, and L. Jain, Comparison between measurements, simulations, and theoretical predictions of the extraction kicker transverse dipole instability in the Spallation Neutron Source, Phys. Rev. ST Accel. Beams **14**, 074401 (2011).
[21] L. J. Laslett, BNL Report No. 7534, 1963, pp. 325–367.
[22] K. Y. Ng, Fermilab Technical Memos Report No. FERMILAB-TM-2152, 2001.
[23] J. A. Holmes, in *Proceedings of the International Particle Accelerator Conference, Kyoto, Japan* (ICR, Kyoto, 2010), pp. 1901–1903.
[24] J. A. Holmes, S. Cousineau, V. V. Danilov, S. Henderson, A. Shishlo, Y. Sato, W. Chou, L. Michelotti, and F. Ostiguy, in *The ICFA Beam Dynamics Newsletter*, Vol. 30 (2003), p. 100.
[25] J. Kamiya, T. Takayanagi, and M. Watanabe, Performance of extraction kicker magnet in a rapid cycling synchrotron, Phys. Rev. ST Accel. Beams **12**, 072401 (2009).
[26] T. Takayanagi, J. Kamiya, M. Watanabe, Y. Yamazaki, Y. Irie, J. Kishiro, I. Sakai, and T. Kawakubo, Design of the injection bump system of the 3-GeV RCS in J-PARC, IEEE Trans. Appl. Supercond. **16**, 1358 (2006).
[27] T. Takayanagi *et al.*, Design and preliminary performance of the new injection shift bump power supply at the J-PARC 3-GeV RCS, IEEE Trans. Appl. Supercond. **24**, 0503504 (2014).
[28] T. Takayanagi *et al.*, Comparison of the pulsed power supply systems using the PFN switching capacitor method and the IGBT chopping method for the J-PARC 3-GeV RCS injection system, IEEE Trans. Appl. Supercond. **24**, 3800905 (2014).
[29] H. Hotchi, N. Tani, Y. Watanabe, H. Harada, S. Kato, K. Okabe, P. K. Saha, F. Tamura, and Y. Yoshimoto, Beam loss caused by edge focusing of injection bump magnets and its mitigation in the 3-GeV rapid cycling synchrotron of the Japan Proton Accelerator Research Complex, Phys. Rev. Accel. Beams **19**, 010401 (2016).
[30] P. K. Saha *et al.*, in *Proceedings of the 4th International Particle Accelerator Conference, IPAC-2013, Shanghai, China, 2013* (JACoW, Shanghai, China, 2013), pp. 521–523.
[31] Y. Watanabe *et al.*, in *Proceedings of the International Particle Accelerator Conference, Kyoto, Japan* (ICR, Kyoto, 2010), pp. 3242–3244.
[32] M. Yoshimoto *et al.*, in *Proceedings of the 2nd International Particle Accelerator Conference, San Sebastián, Spain* (EPS-AG, Spain, 2011), pp. 2412–2414.

[33] J. Kamiya, N. Ogiwara, H. Hotchi, N. Hayashi, and M. Kinsho, Beam loss reduction by magnetic shielding using beam pipes and bellows of solf magnetic materials, Nucl. Instrum Methods Phys. Res., Sect. A **763**, 329 (2014).

[34] P. K. Saha, Y. Shobuda, H. Hotchi, N. Hayashi, T. Takayanagi, H. Harada, and Y. Irie, observation of the phase space footprint of a painting injection in the Rapid Cycling Synchrotron at the Japan Proton Accelerator Research Complex, Phys. Rev. ST Accel. Beams **12**, 040403 (2009).

[35] H. Hotchi *et al.*, Beam loss reduction by injection painting in the 3-GeV rapid cycling synchrotron of the Japan Proton Accelerator Research Complex, Phys. Rev. ST Accel. Beams **15**, 040402 (2012).

[36] P. K. Saha *et al.*, Beam emittance control by changing injection painting area in a pulse-to-pulse mode in the 3-GeV rapid cycling synchrotron of Japan Proton Accelerator Research Complex, Phys. Rev. ST Accel. Beams **16**, 120102 (2013).

[37] F. Tamura *et al.*, Longitudinal painting with large amplitude second harmonic rf voltages in the rapid cycling synchrotron of the Japan Proton Accelerator Research Complex, Phys. Rev. ST Accel. Beams **12**, 041001 (2009).

[38] M. Yamamoto *et al.*, Simulation of longitudinal beam manipulation during multi-turn injection in J-PARC RCS, Nucl. Instrum. Methods Phys. Res., Sect. A **621**, 15 (2010).

[39] N. Hayashi *et al.*, Beam position monitor system of J-PARC RCS, Nucl. Instrum. Methods Phys. Res., Sect. A **677**, 94 (2012).

[40] H. Hotchi, H. Harada, S. Kato, K. Okabe, P. K. Saha, Y. Shobuda, F. Tamura, N. Tani, Y. Watanabe, and M. Yoshimoto, in *Proceedings of the 2017 International Particle Accelerator Conference, IPAC'17, Copenhagen, Denmark* (2017), p. 2470.

[41] S. Igarashi, in *Proceedings of the 57th ICFA Advanced Beam Dynamics Workshop, HB2016, Malmo, Sweden* (JACoW, Malmo, 2016), pp. 21–26.